



# On the use of satellite-derived $\text{CH}_4 : \text{CO}_2$ columns in a joint inversion of $\text{CH}_4$ and $\text{CO}_2$ fluxes

S. Pandey<sup>1,2</sup>, S. Houweling<sup>1,2</sup>, M. Krol<sup>1,2,3</sup>, I. Aben<sup>2</sup>, and T. Röckmann<sup>1</sup>

<sup>1</sup>Institute for Marine and Atmospheric Research Utrecht, Utrecht University, Utrecht, the Netherlands

<sup>2</sup>SRON Netherlands Institute for Space Research, Utrecht, the Netherlands

<sup>3</sup>Wageningen University, Wageningen, the Netherlands

Correspondence to: S. Pandey (s.pandey@uu.nl)

Received: 26 January 2015 – Published in Atmos. Chem. Phys. Discuss.: 24 March 2015

Revised: 13 July 2015 – Accepted: 15 July 2015 – Published: 3 August 2015

**Abstract.** We present a method for assimilating total column  $\text{CH}_4 : \text{CO}_2$  ratio measurements from satellites for inverse modeling of  $\text{CH}_4$  and  $\text{CO}_2$  fluxes using the variational approach. Unlike conventional approaches, in which retrieved  $\text{CH}_4 : \text{CO}_2$  are multiplied by model-derived total column  $\text{CO}_2$  and only the resulting  $\text{CH}_4$  is assimilated, our method assimilates the ratio of  $\text{CH}_4$  and  $\text{CO}_2$  directly and is therefore called the ratio method. It is a dual tracer inversion, in which surface fluxes of  $\text{CH}_4$  and  $\text{CO}_2$  are optimized simultaneously. The optimization of  $\text{CO}_2$  fluxes turns the hard constraint of prescribing model-derived  $\text{CO}_2$  fields into a weak constraint on  $\text{CO}_2$ , which allows us to account for uncertainties in  $\text{CO}_2$ . The method has been successfully tested in a synthetic inversion setup. We show that the ratio method is able to reproduce assumed true  $\text{CH}_4$  and  $\text{CO}_2$  fluxes starting from a prior, which is derived by perturbing the true fluxes randomly. We compare the performance of the ratio method with that of the traditional proxy approach and the use of only surface measurements for estimating  $\text{CH}_4$  fluxes. Our results confirm that the optimized  $\text{CH}_4$  fluxes are sensitive to the treatment of  $\text{CO}_2$ , and that hard constraints on  $\text{CO}_2$  may significantly compromise results that are obtained for  $\text{CH}_4$ . We find that the relative performance of ratio and proxy methods have a regional dependence. The ratio method performs better than the proxy method in regions where the  $\text{CO}_2$  fluxes are most uncertain. However, both ratio and proxy methods perform better than the surface-measurement-only inversion, confirming the potential of spaceborne measurements for accurately determining fluxes of  $\text{CH}_4$  and other greenhouse gases (GHGs).

## 1 Introduction

In the past century, the concentrations of many potent greenhouse gases (GHGs) have increased in the atmosphere due to anthropogenic activities. The atmospheric dry air mole fraction of the greenhouse gas methane ( $\text{CH}_4$ ), which has a global warming potential of 28–34 on a 100-year time horizon (Myhre et al., 2013), has increased from 700 ppb during the pre-industrial era to  $\approx 1800$  ppb today (Ferretti et al., 2005). These atmospheric concentrations are unprecedented during at least the last 650 000 years (Spahni et al., 2005). The direct radiative forcing caused by the increase of methane since pre-industrial times is  $+0.48 \pm 0.05 \text{ W m}^{-2}$  (Myhre et al., 2013), which amounts to 20 % of the present-day cumulative radiative forcing due to all anthropogenic GHGs. Methane also influences atmospheric chemistry and it is an important control on the oxidizing capacity of the atmosphere. Further details about the methane budget can be found in Kirschke et al. (2013). The atmospheric growth rate of methane has varied considerably in the last 2 decades (Bousquet et al., 2006; Nisbet et al., 2014). Causes of these variations are still not fully understood, which calls for better monitoring of its sources and sinks using both top-down and bottom-up studies.

The top-down approach uses inverse modeling techniques to reduce the uncertainty in the bottom-up-derived emission estimates on the basis of atmospheric measurements of  $\text{CH}_4$ . In the past, several studies applied the top-down method assimilating surface-based measurements from global monitoring networks operated by National Oceanic and Atmospheric Administration–Earth System Research Laboratory (NOAA/ESRL), the Advanced Global Atmospheric Gases

Experiment, and the Commonwealth Scientific and Industrial Research Organization (Bousquet et al., 2011, 2006; Hein et al., 1997; Houweling et al., 1999). However, due to poor spatial coverage of the surface measurement sites, such inversions are effective in constraining the fluxes at sub-continental scales at best (Houweling et al., 1999).

Total column measurements of CO<sub>2</sub> and CH<sub>4</sub> ( $X_{\text{CH}_4}$  and  $X_{\text{CO}_2}$ ) from satellites have proven valuable for inversion studies of CH<sub>4</sub> and CO<sub>2</sub>, especially in regions where surface measurement sites are sparse (Basu et al., 2014, 2013; Bergamaschi and Frankenberg, 2009; Houweling et al., 2014). For example, atmospheric retrievals from the Thermal and Near infrared Sensor for carbon Observations (TANSO) onboard the GOSAT (Greenhouse gases Observing SATellite, Kuze et al., 2009) have provided valuable constraints on the fluxes of CH<sub>4</sub> and CO<sub>2</sub> (Basu et al., 2013; Fraser et al., 2013). The CH<sub>4</sub> absorption band at 1.6 micron allows retrieval of its atmospheric concentration with high sensitivity to the planetary boundary layer, where the signals of the sources are strongest. Besides a good sensitivity to the sources, the quality of the inversion-derived CH<sub>4</sub> budget depends strongly on the precision and accuracy of the measurements. It has been shown that systematic errors on regional or seasonal scales of less than 1 % can jeopardize the usefulness of satellite-measured CH<sub>4</sub> columns for estimating CH<sub>4</sub> budget (Bergamaschi et al., 2007).

High-quality  $X_{\text{CH}_4}$  and  $X_{\text{CO}_2}$  retrievals require accurate knowledge of the light path of the photons that are measured by the satellite. Scattering of light by atmospheric particles (aerosol particles and cloud droplets) may lead to significant light-path perturbations. The accuracy of  $X_{\text{CH}_4}$  retrievals depends to a large extent on how well the retrieval technique can account for such scattering-induced perturbations. A commonly used technique is the so-called proxy method, which was originally developed for retrieving  $X_{\text{CH}_4}$  and  $X_{\text{CO}_2}$  using nearby spectral windows from SCIAMACHY (Frankenberg et al., 2005). Since atmospheric scattering affects both compounds in a similar way, light-path errors largely cancel out in the ratio. The retrieval-derived ratio ( $\frac{X_{\text{CH}_4}^{\text{obs}}}{X_{\text{CO}_2}^{\text{obs}}}$ ) is multiplied with a priori knowledge of atmospheric CO<sub>2</sub> derived from a model ( $X_{\text{CO}_2}^{\text{model}}$ ) to generate proxy column measurements of CH<sub>4</sub> ( $X_{\text{CH}_4}^{\text{proxy}}$ ) (Eq. 1).

$$X_{\text{CH}_4}^{\text{proxy}} = \frac{X_{\text{CH}_4}^{\text{obs}}}{X_{\text{CO}_2}^{\text{obs}}} \times X_{\text{CO}_2}^{\text{model}} \quad (1)$$

$X_{\text{CO}_2}^{\text{model}}$  is usually derived from the results of a CO<sub>2</sub> inversion using the surface measurements, such as CarbonTracker (Peters et al., 2007). It is assumed that (1) CO<sub>2</sub> exhibits comparatively smaller unknown variations in the atmosphere than CH<sub>4</sub>, and (2) residual differences in scattering between the spectral windows of CO<sub>2</sub> (1562 to 1585 nm) and CH<sub>4</sub> (1630 to 1670 nm) used in the retrieval are insignificant.

Hence, CO<sub>2</sub> is used as proxy for changes in the light path. Schepers et al. (2012) discuss the performance of GOSAT RemoTeC proxy retrieval in detail. This retrieval data set has been used successfully in inversion studies for optimizing CH<sub>4</sub> fluxes (Alexe et al., 2015; Monteil et al., 2013). In these studies the error in  $X_{\text{CO}_2}^{\text{model}}$  is assumed to be negligible compared to retrieval error in  $\frac{X_{\text{CH}_4}^{\text{obs}}}{X_{\text{CO}_2}^{\text{obs}}}$ . However, with the gradually improving quality of the GOSAT retrievals, errors in model-derived CO<sub>2</sub> may become a bottleneck for improving inversion-derived CH<sub>4</sub> fluxes (Schepers et al., 2012).

In some regions, the sparse network of surface measurement sites does not provide sufficient constraints on CO<sub>2</sub> fluxes, leading to possible biases in  $X_{\text{CO}_2}^{\text{model}}$  (Schepers et al., 2012). In this study we investigate a new method, called the ratio method, which circumvents the use of  $X_{\text{CO}_2}^{\text{model}}$  by directly assimilating the retrieved ratio of total column CH<sub>4</sub> and CO<sub>2</sub> into an inversion that optimizes CH<sub>4</sub> and CO<sub>2</sub> fluxes simultaneously. Thus, in the ratio method, Eq. (1) is replaced with

$$X_{\text{ratio}} = \frac{X_{\text{CH}_4}^{\text{obs}}}{X_{\text{CO}_2}^{\text{obs}}} \quad (2)$$

Our motivation for implementing the ratio method is to find a representation of CO<sub>2</sub> in the inversion system that is more consistent with both  $X_{\text{ratio}}$  and CO<sub>2</sub> surface measurements. Also,  $X_{\text{ratio}}$  is less biased and has a larger number of measurements than  $X_{\text{CH}_4}$  and  $X_{\text{CO}_2}$  full-physics retrievals (Fraser et al., 2014). Fraser et al. (2014) introduced the assimilation of satellite retrieved  $X_{\text{ratio}}$  in a maximum a posteriori (MAP) inversion system for constraining the surface fluxes of CH<sub>4</sub> and CO<sub>2</sub>. However, the transport model and inversion method used in their study are different from the ones used here.

We perform observing system simulation experiments (OSSEs) to test the performance of the ratio method for reproducing the assumed true fluxes of CH<sub>4</sub> and CO<sub>2</sub>. The results are compared with inversions using proxy retrievals and only surface measurements. In the following section, we elaborate on our inverse modeling setup, and describe our OSSE experiments. In Sect. 3, we analyze and compare the inversion-estimated posterior fluxes of CH<sub>4</sub> and CO<sub>2</sub>. In Sect. 4, we further discuss the significance and limitations of our findings and evaluate the future potential of the ratio method for application in inversion studies, leading to our final conclusions.

## 2 Method

### 2.1 Inverse modeling

We use the TM5-4DVAR inversion system in this study. It is comprised of the Tracer Transport Model version 5 (TM5, Krol et al., 2005) coupled to a variational data assimilation

system (4DVAR, Meirink et al., 2008). TM5 simulates the spatiotemporal distribution of a tracer in the atmosphere for a given set of fluxes and initial concentrations that are prescribed as boundary conditions to the model. We have set up a dual tracer version of TM5-4DVAR for simultaneous simulation of CH<sub>4</sub> and CO<sub>2</sub>. By combining the output of the two tracers, this model allows us to simulate  $X_{\text{ratio}}$  (see Eq. 2). The 4DVAR technique uses the model-calculated and observational data set of  $X_{\text{ratio}}$  to optimize a state vector  $\mathbf{x}$ , consisting of surface fluxes of CH<sub>4</sub> and CO<sub>2</sub>. The optimum is found by minimizing a Bayesian cost function, defined as

$$J(\mathbf{x}) = \frac{1}{2}(\mathbf{x} - \mathbf{x}_b)^T \mathbf{B}^{-1}(\mathbf{x} - \mathbf{x}_b) + \frac{1}{2}(\mathbf{y} - \mathbf{H}\mathbf{x})^T \mathbf{R}^{-1}(\mathbf{y} - \mathbf{H}\mathbf{x}), \quad (3)$$

where  $\mathbf{x}_b$  is the a priori knowledge of  $\mathbf{x}$ , and  $\mathbf{H}$  is the observation operator, which converts the output of the model, forced by  $\mathbf{x}$ , to corresponding mixing ratios at the measurement sites of  $\mathbf{y}$ . Hence,  $\mathbf{H}\mathbf{x}$  represents the model-simulated counterpart of the observation vector  $\mathbf{y}$ .  $\mathbf{R}$  and  $\mathbf{B}$  are error covariance matrices for  $\mathbf{y} - \mathbf{H}\mathbf{x}$  and  $\mathbf{x}_b$ , respectively. Each iteration of TM5-4DVAR is composed of a forward and an adjoint TM5 run (Errico, 1997). The forward run is used to calculate the value of the cost function for a trial state vector  $\mathbf{x}_j$  (using Eq. 3). The adjoint run provides the corresponding cost function gradient ( $\nabla J(\mathbf{x}_j)$ ). At the end of each inversion iteration  $j$ ,  $\nabla J(\mathbf{x}_j)$  and the state vector  $\mathbf{x}_j$  are fed into an optimizer module to calculate the state vector for the next iteration ( $\mathbf{x}_{j+1}$ ). For linear inverse problems we use the conjugate gradient optimizer (CONGRAD, Lanczos, 1950), which has been used extensively for linear inversion problems (Basu et al., 2013; Houweling et al., 2014; Monteil et al., 2011, 2013). Mathematically, it has the fastest convergence rate for linear inversions, but it may perform poorly for nonlinear inversions.

Our inversion setup for the proxy approach is linear. However, for the new ratio method the operator  $\mathbf{H}$  includes Eq. (2), and hence, the inversion becomes nonlinear making M1QN3 a more suitable optimizer than CONGRAD. M1QN3 is a quasi-Newtonian algorithm-based optimizer (Gilbert and Lemaréchal, 1989), which is commonly used in nonlinear inverse modeling (Cressot et al., 2014; Krol et al., 2013; Müller and Stavrou, 2005). It has the ability to rebuild the second derivative of the cost functions several times during its descent to minimum, and therefore, performs better for nonlinear inverse problems.

To compare the difference in convergence between M1QN3 and CONGRAD, we performed additional proxy inversions using both optimization methods (see Appendix A). We find that M1QN3 has a slower convergence rate in comparison to CONGRAD, and therefore the number of iterations needed to find the inversion solution is generally higher. Another drawback of the M1QN3 algorithm available to us

**Table 1.** Covariance parameters of the a priori flux uncertainties per grid box per month used in the inversions. The uncertainty is expressed as a fraction of the a priori flux. Error correlations are defined by exponential (“e”) and Gaussian (“g”) correlation functions using the specified length scales (Basu et al., 2013).

| Tracer category           | Uncertainty (%) | Temporal (months) | Spatial (km) |
|---------------------------|-----------------|-------------------|--------------|
| CH <sub>4</sub> Total     | 50              | 3.0 e             | 500.0 g      |
| CO <sub>2</sub> Biosphere | 250             | 3.0 e             | 1000.0 g     |
| CO <sub>2</sub> Ocean     | 250             | 6.0 e             | 1000.0 g     |

is that, unlike CONGRAD, it provides no information about the posterior flux uncertainties in a straightforward way.

## 2.2 Truth and prior

The assumed true CH<sub>4</sub> and CO<sub>2</sub> fluxes for our inversion setup are taken as the a priori fluxes used by Houweling et al. (2014) and Basu et al. (2013), respectively. The generation of pseudo-observations  $\mathbf{y}$  is explained in the next section. Concerning the state vector  $\mathbf{x}$ , CH<sub>4</sub> fluxes are optimized for a single category representing the net flux from all the contributing processes at the surface, discretized per model grid box and per month. For CO<sub>2</sub>, we optimize for fluxes from the biosphere and the ocean, discretized in time and space like methane. We do not optimize emissions from other categories like biomass burning and fossil fuel usage, as they are assumed to have relatively small uncertainties. Table 1 shows the parameters used to calculate the error covariance matrix  $\mathbf{B}$  for the prior fluxes. We assume no prior correlation between flux categories of CO<sub>2</sub> biosphere, CO<sub>2</sub> oceanic and CH<sub>4</sub> total. The spatiotemporal covariance components for each category were included in  $\mathbf{B}$ . For details about this implementation of  $\mathbf{B}$  in our inversion, see Basu et al. (2013). We use one set of prior fluxes  $\mathbf{x}_b$  for all inversions, which was created by adding Gaussian noise to the true CH<sub>4</sub> and CO<sub>2</sub> fluxes. The noise is generated using the a priori flux uncertainties accounting for spatial and temporal error correlations, as described in Chevallier et al. (2007). Figure 2 shows the time series of the true and prior fluxes for four Transcom regions (explained in Fig. 1). As can be seen, the assumptions regarding the a priori flux uncertainties lead to realistic deviations from the truth in terms of seasonality and net monthly flux.

## 2.3 Measurements

Pseudo-surface observations are generated from a forward run of TM5 using the “true” fluxes as boundary conditions, and they are sampled at coordinates and times of samples collected by cooperative flask-sampling network run by NOAA/ESRL (Dlugokencky et al., 2009) in the period 1 June 2009 to 30 May 2010 at the sites shown in Fig. 1. In

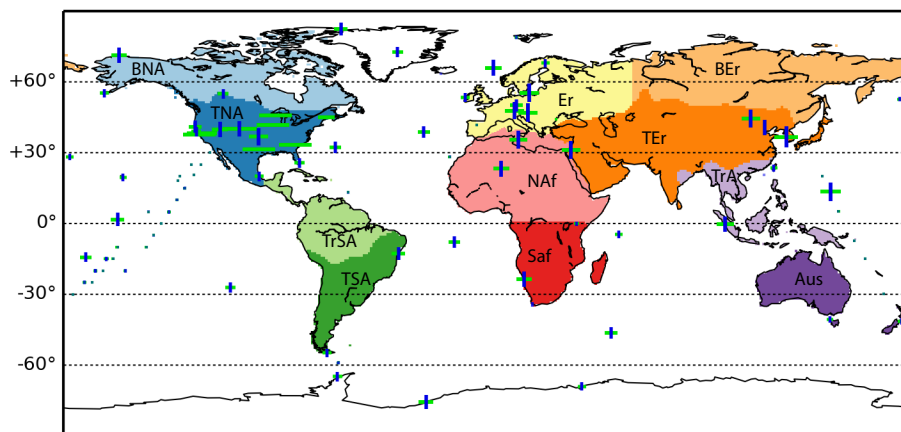


**Figure 1.** The dynamic symbols (blue–green crosses) show the location of the NOAA measurements sites included in inversions using surface measurements (see Table 2). The lengths of vertical blue and horizontal green bars are proportional to the number of CO<sub>2</sub> and CH<sub>4</sub> measurements, respectively. Continents are divided into 11 Transcom land regions (Gurney et al., 2002) which will be referred to in Sects. 4 and 3 as: Boreal North America (BNA), Temperate North America (TNA), Tropical South America (TrSA), Temperate South America (TSA), Northern Africa (NAf), Southern Africa (Saf), Boreal Eurasia (BEr), Temperate Eurasia (TEr), Tropical Asia (TrAs), Australia (Aus), and Europe (Eur).

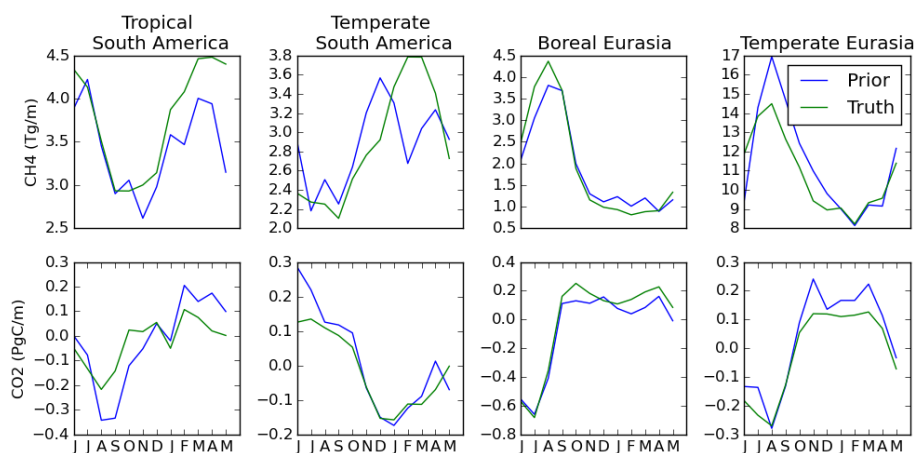


**Figure 2.** Time series of the true and prior fluxes (per month) integrated over Tropical South America, Temperate South America, Boreal Eurasia and Temperate Eurasia. For CH<sub>4</sub>, we show the total fluxes, and for CO<sub>2</sub>, we show the biosphere fluxes (see Table 1).

total, we use 3934 surface measurements of CH<sub>4</sub> (from 93 sites) and 1184 measurements of CO<sub>2</sub> (from 85 sites). Similarly, synthetic total column measurements are generated at the times and locations of the GOSAT RemoTeC v1.9 proxy satellite retrievals for the same time period (Schepers et al., 2012). We do not sample GOSAT data for cloud free conditions, and therefore assimilate a rather optimistic number of GOSAT measurements. However, satellites such as Sentinel-5 will provide a comparable amount of data. The forward run of TM5 calculates 25-layer vertical model profiles at the retrieval coordinates. These profiles are converted into the corresponding total columns using the retrieval-derived averaging kernels (see e.g., Monteil et al., 2013). In total, we use 443 523 GOSAT total column retrievals of both CH<sub>4</sub> and CO<sub>2</sub> (see Fig. 3).

The observational part of the cost function is calculated by weighing the mismatch between the model simulations and measurements ( $y - Hx$ ) with the data error covariance matrix  $\mathbf{R}$ . The diagonal terms of  $\mathbf{R}$  are the squared sum of measurement uncertainty and model representation error. The model representation error is the error made by our finite resolution model in simulating a sample at a specific location. Its size scales with the subgrid concentration variability, and is calculated using the local concentration gradient simulated by the model. Further details about the calculation of the model representation error in our setup can be found in Basu et al. (2013). For the measurement uncertainties, we follow the recommendations of the data providers. For the GOSAT retrieved total column ratios, the uncertainty was calculated by error propagation of the instrument's measurement noise

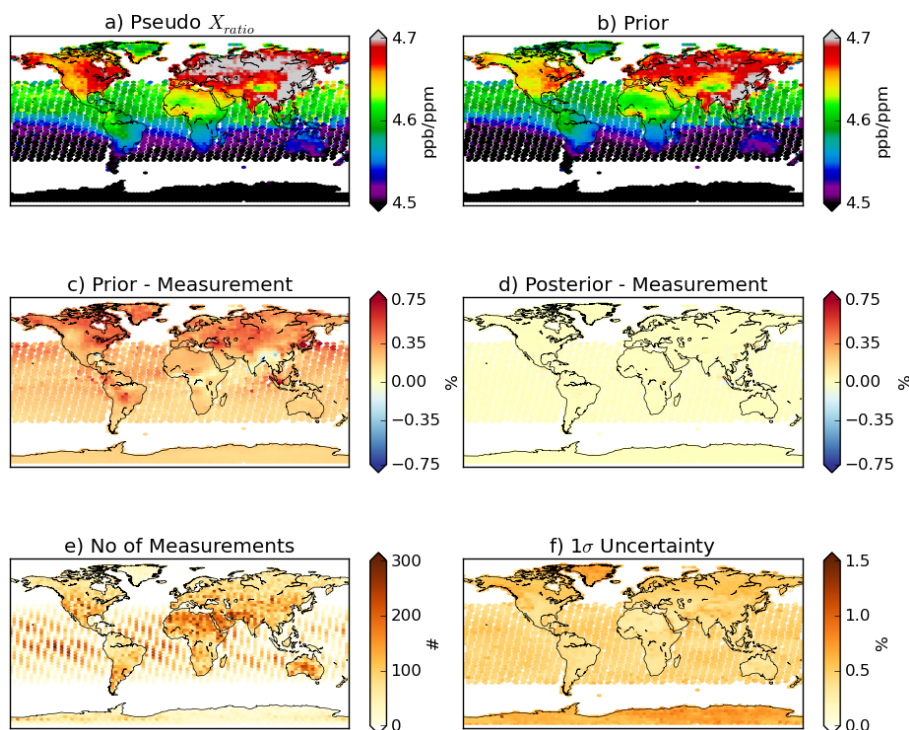


**Figure 3.** Fit of the RATIO inversion to the annually averaged “true”  $X_{ratio}$  pseudo-measurements. (a) True  $X_{ratio}$  pseudo-measurements, (b) a priori-modeled  $X_{ratio}$ , (c) mismatch between the a priori model and the pseudo-data, (d) the corresponding mismatch of the posterior model, (e) the number of GOSAT measurements, (f) the 1 $\sigma$  data uncertainty of  $X_{ratio}$ . The values represent yearly averages per  $6^\circ \times 4^\circ$  (latitude  $\times$  longitude) grid box, except the bottom left panel which shows yearly integrals over  $6^\circ \times 4^\circ$  (latitude  $\times$  longitude).

of the CH<sub>4</sub> and CO<sub>2</sub> total columns given in retrieval data set. The uncertainties of proxy CH<sub>4</sub> total columns are also calculated in similar ways. In principle, they should be the ratio uncertainties plus the  $X_{CO_2}^{model}$  uncertainty (see Eqs. 1 and 2). However, the uncertainties from  $X_{CO_2}^{model}$  are neglected in real world applications, and we follow the same procedure. Hence, in our experiment, the ratio and proxy columns have the same relative uncertainties. For computational efficiency, we assume no correlation between the measurements (i.e., all the non-diagonal term of  $\mathbf{R}$  are set to zero).

Formally, we should perturb the pseudo-measurements with noise according to the data covariance matrix  $\mathbf{R}$ , following the same procedure as for the a priori fluxes. However, to catch the mean behavior one would have to do several inversions with different noise realizations. This multi-inversion mean would correspond to the results of a single inversion without noise. For this reason we do not perturb the data. It should also be noted that satellite measurements are simulated using the same prior profiles as used for the real RemoTeC GOSAT retrievals. Since the same prior profile is used in the inversion and in the generation of pseudo-data, its contribution cancels out in the model data mismatch and therefore does not influence the results.

In the ratio inversion, the GOSAT measurements are in terms of  $X_{ratio}$ , whereas the output of the transport model

is in terms of  $X_{CH_4}^{obs}$  and  $X_{CO_2}^{obs}$ . The observation operator  $\mathbf{H}$  transforms the absolute columns to column ratios using Eq. (2). For calculating the gradient of  $J(\mathbf{x})$ , the adjoint of  $\mathbf{H}$  is needed for propagating the sensitivities of the cost function from  $X_{ratio}$  to the corresponding sensitivities of  $X_{CH_4}^{obs}$  and  $X_{CO_2}^{obs}$ . This adjoint is derived by applying the adjoint coding rules described in Errico (1997). It should be noted that the problem is only weakly nonlinear since the values of  $X_{CO_2}^{obs}$  vary in the narrow range of  $\approx 350$ – $400$  ppm in our calculations, and the inversion-derived adjustments to  $X_{CO_2}^{obs}$  are only a small fraction of that range.

## 2.4 Experiment

In this study, we perform OSSEs comparing different global inversion setups using the same truth and a priori fluxes. The inversions system is run at a  $6^\circ \times 4^\circ$  horizontal resolution and 25 vertical hybrid sigma pressure levels from the surface to the top of the atmosphere. Simulations are performed for the period 1 June 2009 to 30 May 2010. The transport in TM5 is driven by meteorological fields from the European Centre for Medium-Range Weather Forecasts (ECMWF) ERA-Interim reanalysis project (Dee et al., 2011). Table 2 provides an overview of the inversions that have been performed, specifying the fluxes that were optimized, the optimizer that was

**Table 2.** Summary of the inversions performed in this study.

| Inversion | Measurements   | Fluxes optimized                  | Optimizer (no. of iterations) |
|-----------|--|-----------------------------------|-------------------------------|
| RATIO     | $X_{\text{ratio}}$ , surface CH <sub>4</sub> , CO <sub>2</sub> | CH <sub>4</sub> , CO <sub>2</sub> | M1QN3 (100)                   |
| SURFCO2   | surface CO <sub>2</sub>  | CO <sub>2</sub>                   | CONGRAD (50)                  |
| PROXY     | $X_{\text{CH}_4}^{\text{proxy}}$ , surface CH <sub>4</sub>     | CH <sub>4</sub>                   | CONGRAD (50)                  |
| SURFCH4   | surface CH <sub>4</sub>  | CH <sub>4</sub>                   | CONGRAD (50)                  |
| TRU-DAT   | $X_{\text{CH}_4}^{\text{proxy}}$ , surface CH <sub>4</sub>     | CH <sub>4</sub>                   | CONGRAD (50)                  |
| PRICO2    | $X_{\text{CH}_4}^{\text{proxy}}$ , surface CH <sub>4</sub>     | CH <sub>4</sub>                   | CONGRAD (50)                  |

used with number of iterations, and the type of measurements assimilated. The PROXY inversion requires  $X_{\text{CO}_2}^{\text{model}}$  (see Eq. 1), which is calculated by sampling the output of a forward run of TM5 using posterior CO<sub>2</sub> fluxes from the SURFCO2 inversion and applying the GOSAT averaging kernel.

The TRU-DAT represents an inversion which assumes that we have perfect knowledge of  $X_{\text{CO}_2}^{\text{model}}$ . It is used as a best-case scenario for the proxy method. In contrast,  $X_{\text{CO}_2}^{\text{model}}$  for PRICO2 was calculated using prior CO<sub>2</sub> fluxes transformed directly into observations using TM5 without optimization using CO<sub>2</sub> surface measurements. This inversion represents a worst case scenario for the proxy method. The RATIO inversion uses our new ratio method, assimilating surface CH<sub>4</sub> and CO<sub>2</sub> observations, and  $X_{\text{ratio}}$  for optimizing surface CH<sub>4</sub> and CO<sub>2</sub> fluxes. PROXY represents the common use of proxy retrievals in atmospheric inverse modeling. In PROXY, the same amount of measurements are assimilated in a series of two linear inversions: (1) optimization of CO<sub>2</sub> fluxes with surface observations (SURFCO2), (2) an inversion using surface CH<sub>4</sub> and  $X_{\text{CH}_4}^{\text{proxy}}$  (PROXY). We use 50 iterations of CONGRAD for both of these inversions. In RATIO, all the information is assimilated in a single inversion using 100 iteration of M1QN3.

## 2.5 Analysis

In Sect. 3, we analyze the monthly time series of posterior fluxes from different inversions using Taylor plots (Taylor, 2001) and mean annual departures from the true fluxes aggregated over the Transcom land regions. We define the following parameters to represent the average deviation of the posterior fluxes from the truth over all the Transcom land regions:

$$\begin{aligned}\kappa &= \overline{|\text{cor} - 1|}, \\ \gamma &= \overline{|\sigma/\sigma_{\text{truth}} - 1|}, \\ \beta &= \overline{|\text{bias}|},\end{aligned}\quad (4)$$

**Table 3.**  $\kappa$ ,  $\gamma$  and  $\beta$  values of the inversions performed in this study (see Eq. 4 and Table 2). The  $\beta$  values have a unit of Tg yr<sup>-1</sup> for CH<sub>4</sub> and Pg C yr<sup>-1</sup> for CO<sub>2</sub>.  $\kappa$  and  $\gamma$  are unitless quantities.

| Tracer          | Inversion | $\kappa$ | $\gamma$ | $\beta$ |
|-----------------|-----------|----------|----------|---------|
| CH <sub>4</sub> | PRIOR     | 0.286    | 0.211    | 2.370   |
|                 | RATIO     | 0.122    | 0.129    | 1.396   |
|                 | PROXY     | 0.119    | 0.137    | 1.432   |
|                 | SURFCH4   | 0.218    | 0.162    | 1.959   |
|                 | TRU-DAT   | 0.024    | 0.042    | 0.621   |
|                 | PRICO2    | 0.210    | 0.258    | 2.409   |
| CO <sub>2</sub> | PRIOR     | 0.232    | 0.392    | 0.327   |
|                 | SURFCO2   | 0.180    | 0.241    | 0.185   |
|                 | RATIO     | 0.125    | 0.225    | 0.134   |

where cor is the cross-correlation between the posterior and true monthly flux time series for a Transcom region, and  $\sigma/\sigma_{\text{truth}}$  is the relative SD of the posterior and true monthly flux time series of a Transcom region. In the Taylor plots,  $\sigma/\sigma_{\text{truth}} = 1$  and cor = 1 represent the true fluxes and therefore, we subtract 1 from both the values in Eq. (4) to represent the deviation of prior or posterior fluxes from true fluxes. Finally, bias is the difference between the posterior and true net annual flux of a Transcom region. It should be noted that  $\kappa$  and  $\gamma$  are dimensionless, and  $\beta$  has a unit of Tg yr<sup>-1</sup> for CH<sub>4</sub> and Pg C yr<sup>-1</sup> for CO<sub>2</sub>. Table 3 lists the values of these parameters for the inversions performed in this study. The closer these values are to zero for an inversion, the better it is performing. With each parameter at zero the agreement between the true and inversion-optimized fluxes is perfect.

## 3 Results

### 3.1 Ratio method implementation

Figure 3 summarizes the performance of RATIO (see also Table 2). The pseudo- $X_{\text{ratio}}$  measurements have typical values in the range of 4.4 to 4.8 ppb ppm<sup>-1</sup>. We observe that the latitudinal gradient of CH<sub>4</sub> atmospheric concentration is

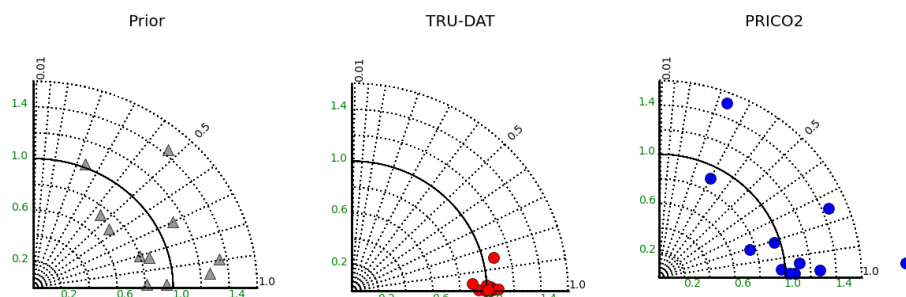


**Figure 4.** Taylor plots (Taylor, 2001) of monthly prior (grey triangles) and posterior CH<sub>4</sub> fluxes integrated over 11 Transcom land regions for the inversions TRU-DAT (red circles) and PRICO2 (blue circles). In these plots, each dot represents a seasonal variation of a single Transcom region. The true fluxes are at the intersection point of the  $x$  axis and the bold arc (representing a  $\text{cor} = 1$  and  $\sigma/\sigma_{\text{truth}} = 1$ ).

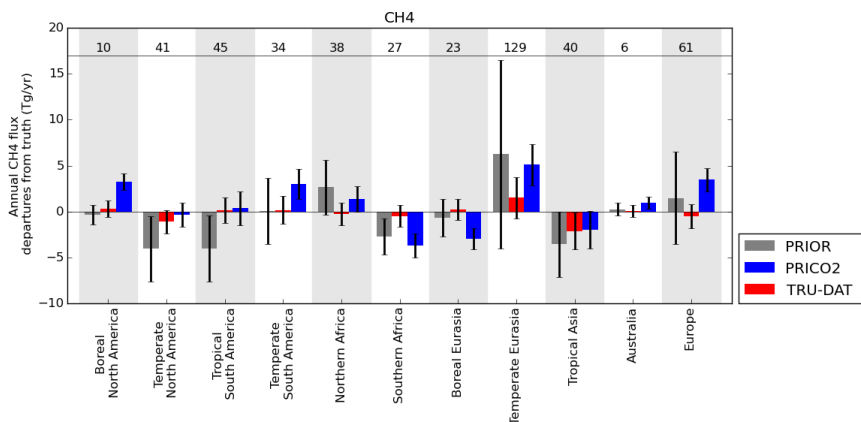


**Figure 5.** Annual prior and posterior CH<sub>4</sub> flux departures from the true fluxes for the Transcom land regions for the inversions TRU-DAT and PRICO2. The true fluxes are written at the top of the plot in Tg yr<sup>-1</sup>. The vertical black lines on the bars show 1 $\sigma$  uncertainty of the corresponding values.

a dominant mode of variation in  $X_{\text{ratio}}$ . The randomly generated globally and annually integrated a priori CO<sub>2</sub> flux, combining land and ocean, is 2.01 Pg C yr<sup>-1</sup> larger than the true flux (truth = -4.65 Pg C yr<sup>-1</sup>, prior = -2.640 Pg C yr<sup>-1</sup>). As a result of this, the a priori fluxes overestimate the global CO<sub>2</sub> increase. The global annual prior CH<sub>4</sub> flux is only 6.85 Tg yr<sup>-1</sup> lower than the truth (truth = 541.764 Tg yr<sup>-1</sup>, prior = 534.905 Tg yr<sup>-1</sup>), which is a much smaller relative deviation from the true fluxes compared to CO<sub>2</sub>. Hence, the percentage mismatch between the modeled prior and measured  $X_{\text{ratio}}$  is mostly positive over the globe (Fig. 3c). The figure also compares the prior and posterior misfits of RATIO to the “true”  $X_{\text{ratio}}$ . The measurement uncertainty of  $X_{\text{ratio}}$  increases towards higher latitudes. We find a gradient norm reduction of  $\approx 2000$  for 100 iterations of MIQN3. As expected, the posterior mismatches are strongly reduced in comparison to the prior, demonstrating that the ratio inversion system works mathematically and that it is reasonably efficient in minimizing the cost function. The improved fit of measurements also leads to a convergence of the posterior fluxes towards the true fluxes, as will be discussed in detail in Sect. 3.3 and 3.4.

### 3.2 TRU-DAT and PRICO2

As explained in Sect. 2.4, TRU-DAT and PRICO2 represent best and worst case scenarios of the impact of errors in  $X_{\text{CO}_2}^{\text{model}}$  on the results of a proxy inversion. Here we analyze the differences between these inversions, which inform us about the sensitivity of the proxy method to errors in  $X_{\text{CO}_2}^{\text{model}}$ . Figure 4 compares the performance of PRICO2 and TRU-DAT using Taylor plots. In these plots, each point represents a 12-month time series of CH<sub>4</sub> fluxes integrated over a Transcom land region. Compared to the prior ( $\kappa = 0.286$  and  $\gamma = 0.211$ ), the posterior fluxes of TRU-DAT shows much better agreement with the true fluxes ( $\kappa = 0.024$  and  $\gamma = 0.042$ ). PRICO2 ( $\kappa = 0.210$  and  $\gamma = 0.258$ ), on the other hand, performs even worse than the prior in terms of  $\gamma$ . Figure 5 shows how well the TRU-DAT and PRICO2 inversions are capable of reproducing the true annual fluxes integrated over Transcom land regions. The  $\beta$  values are 2.370, 2.409 and 0.621 Tg yr<sup>-1</sup> for PRIOR, PRICO2 and TRU-DAT, respectively. Again, we observe that on average the results of TRU-DAT are closest to the truth, and that the results for PRICO2 are further away from truth than the a priori fluxes.

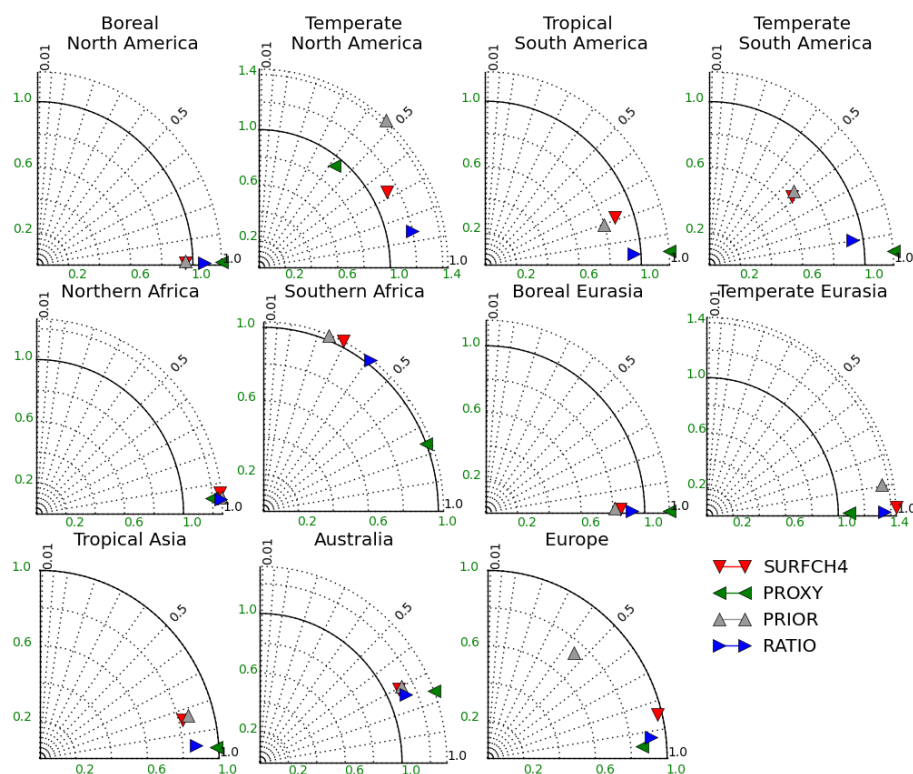


**Figure 6.** As Fig. 4 for the RATIO, PROXY and SURFCH4 inversions.

This tells us that the performance of inversions assimilating proxy data is sensitive to our knowledge of the CO<sub>2</sub> fluxes. In practical applications, however, the CO<sub>2</sub> fluxes will first be optimized using surface measurements to obtain a better representation of atmospheric CO<sub>2</sub> concentrations. Inversions representing this approach will be discussed in the next section.

### 3.3 PROXY, RATIO and SURFCH4

Next we analyze the difference between the proxy inversion (PROXY), using optimized CO<sub>2</sub> concentrations from SURFCO<sub>2</sub>, and our new ratio method (RATIO). For comparison, we also include results of SURFCH<sub>4</sub> using only surface CH<sub>4</sub> measurements. The performance of these inversions is analyzed as in Sect. 3.2, and the results are summarized in Figs. 6 and 7. All three inversions improve the cor of the posterior fluxes with the truth compared to the prior but have varied performance in improving  $\sigma/\sigma_{\text{truth}}$ . The prior fluxes of Boreal North America are closer to the truth than any of the posterior fluxes. However, it should be noted that the prior fluxes were created by adding random noise to the truth, which happens to be a small perturbation occasionally. This is why we average results over all Transcom land regions to derive meaningful comparisons. The  $\kappa$  and  $\gamma$  values, representing the average performance over Transcom land regions, are shown in Table 3. We observe that RATIO and PROXY

perform better than SURFCH<sub>4</sub>, confirming the importance of information provided by the satellite measurements.

Figure 7 shows the departures of the annual fluxes from the truth aggregated over Transcom land regions. The  $\beta$  values are 2.37, 1.40, 1.43, and 1.96 Tg yr<sup>-1</sup> for PRIOR, RATIO, PROXY, and SURFCH<sub>4</sub>, respectively (see Table 3). Overall, we find that the performance of RATIO and PROXY is similar. RATIO performs better than PROXY in six regions, and PROXY is better in the other five regions. The PROXY inversion shows the worst performance in Boreal North America, Temperate North America and Boreal Eurasia, and RATIO has the worst performance in Southern Africa.

We find that with the additional information provided by the satellite measurements RATIO and PROXY are able to reproduce the true fluxes better than SURFCH<sub>4</sub>. However, it is difficult to conclude if RATIO or PROXY performs better, as their relative performances vary across the regions. As can be seen in Figs. 6 and 7, PROXY clearly performs poorly over Temperate North America. Similarly, RATIO performs worse in Southern Africa than PROXY. These varying relative performances are further investigated in the next subsection. Annual flux uncertainties of the fluxes are shown as error bars in Fig. 7. It should be noted that unlike PROXY and SURFCH<sub>4</sub>, RATIO does not estimate posterior uncertainties. This drawback of RATIO will be further discussed in Sect. 4. The reduction in uncertainty is larger for PROXY than SURFCH<sub>4</sub> in the regions where we have less surface measure-

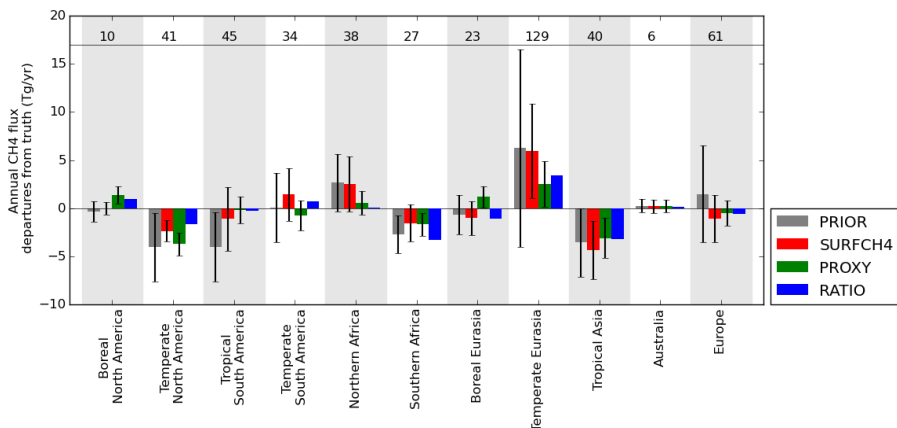


Figure 7. As Fig. 5 for RATIO, PROXY and SURFCH4.

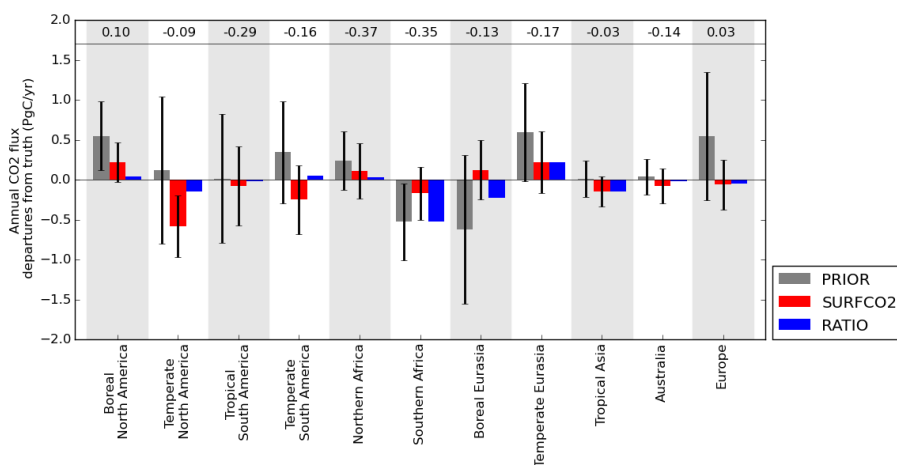


Figure 8. As Fig. 5 for the biosphere CO<sub>2</sub> fluxes in RATIO and SURFCO<sub>2</sub> inversions.

ments (in Tropical South America, Temperate South America, Northern Africa). This can be attributed to the larger number of satellite observations in comparison to surface measurements in these regions. In other regions, both inversions show similar uncertainty reductions due to a higher gradient norm reduction achieved by SURFCH<sub>4</sub> ( $3.1 \times 10^{10}$ ) compared to PROXY ( $3.9 \times 10^3$ ). Both inversions are run for 50 iterations, but PROXY has a larger number of data to assimilate than SURFCH<sub>4</sub>, and therefore, it achieves a lower gradient norm reduction.

### 3.4 CO<sub>2</sub> fluxes

As explained in Sect. 1, the motivation for our ratio technique is to obtain a more consistent representation of the CO<sub>2</sub> concentration fields in the atmosphere. In this subsection, we address the question whether RATIO optimized CO<sub>2</sub> fluxes are indeed closer to the truth than those obtained using SURFCO<sub>2</sub> (which are used for PROXY). Figure 8 shows the deviations of posterior CO<sub>2</sub> fluxes from the truth for RATIO and

SURFCO<sub>2</sub>. In general, annual a priori CO<sub>2</sub> fluxes show large relative deviations from the truth compared to CH<sub>4</sub>. This is a direct consequence of the assumed a priori flux uncertainties (see Table 1). The  $\beta$  values (Table 3) are 0.327, 0.185 and  $0.134 \text{ PgC yr}^{-1}$  for PRIOR, SURFCO<sub>2</sub> and RATIO, respectively. RATIO is able to constrain CO<sub>2</sub> fluxes better than SURFCO<sub>2</sub>. The difference between SURFCO<sub>2</sub> and RATIO is explained by regions such as Temperate North America and Temperate South America, which are relatively poorly constrained by SURFCO<sub>2</sub>. In Temperate North America, due to coarse resolution of the model in combination with large emission gradients, large representation errors are assigned to the simulated measurements. Also, we do not take full advantage of surface measurement coverage of this region as we use only fully processed NOAA/ESRL flask measurements. A lack of surface measurements could be the reason for the poor performance of SURFCO<sub>2</sub> in Temperate South America. We observe that RATIO performs better in these regions with the help of satellite measurements.

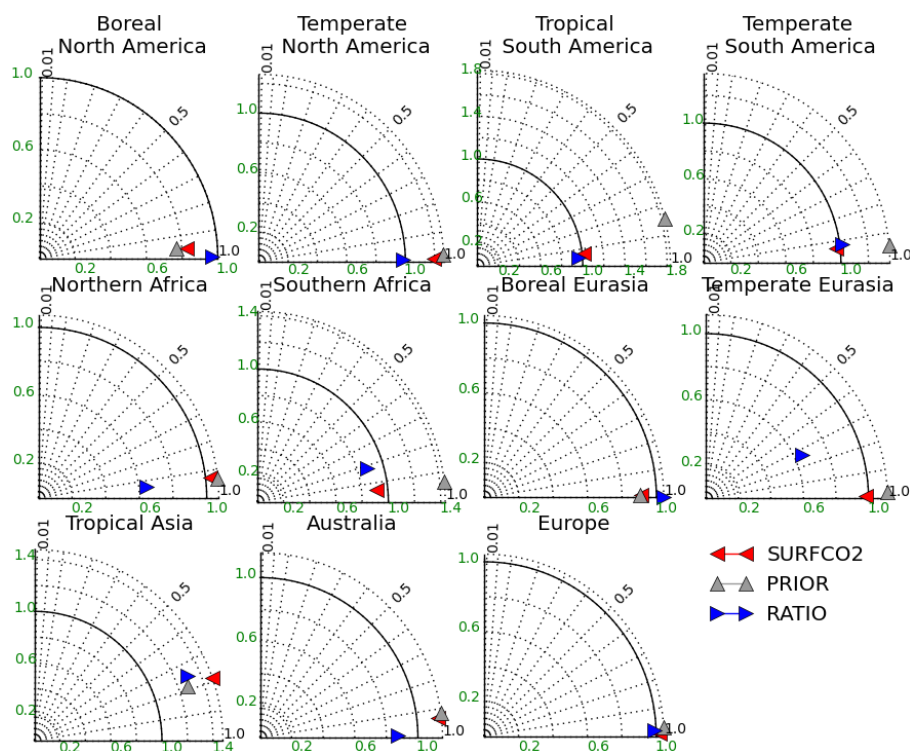


**Figure 9.** As Fig. 4 for the biosphere CO<sub>2</sub> fluxes in RATIO and SURFCO2 inversions.

Figure 9 shows how well the inversion-derived CO<sub>2</sub> fluxes reproduce the true seasonality. Compared with CH<sub>4</sub>, the prior fluxes correlate well with the truth, despite their relatively large a priori uncertainties. This reflects the large seasonal variation in the biospheric CO<sub>2</sub> fluxes. For CO<sub>2</sub>, the differences in the Taylor diagrams are dominated by variations in  $\sigma/\sigma_{\text{truth}}$ . Overall, RATIO ( $\kappa = 0.125$ ,  $\gamma = 0.225$ ) performs better than SURFCO2 ( $\kappa = 0.180$ ,  $\gamma = 0.241$ ). RATIO is able to reproduce the true seasonality for most regions except Northern Africa, Temperate Eurasia and Tropical Asia. In Temperate Eurasia, SURFCO2 performs very well. However, it performs worse than RATIO in Tropical Asia. In Tropical South America and Temperate South America, we find a similar performance of RATIO and SURFCO2. The prior for Europe does not deviate much from the truth, so the relative performance for the two methods cannot be judged adequately.

### 3.5 The link between CO<sub>2</sub> and CH<sub>4</sub>

In principle, the performance of PROXY should improve with the performance of SURFCO2. If SURFCO2 reproduces the true CO<sub>2</sub> fluxes exactly, the only source of error in  $X_{\text{CH}_4}^{\text{proxy}}$  due to  $X_{\text{CO}_2}^{\text{model}}$  will be the representation error of the finite resolution model used for generating spatiotemporal fields of CO<sub>2</sub>. Also in the case of RATIO, the correctness of posterior CH<sub>4</sub> fluxes is dependent upon the correctness of CO<sub>2</sub> fluxes and vice versa. For example, Figs. 8 and 9

show RATIO performs poorly for Southern Africa, and that SURFCO2 performs poorly for Temperate North America for constraining CO<sub>2</sub> fluxes. This is also reflected in the poor performance of RATIO and PROXY in constraining CH<sub>4</sub> fluxes in these regions (Sect. 3.3). The performance of SURFCO2 varies regionally, which causes a corresponding pattern in the performance of PROXY. The same relation should hold for the posterior CO<sub>2</sub> and CH<sub>4</sub> fluxes calculated with RATIO. To quantify this relation, we define  $p_{\text{CH}_4}$  as a measure of the relative accuracy of RATIO- and PROXY-derived CH<sub>4</sub> fluxes, and  $p_{\text{CO}_2}$  as a measure of the relative accuracy of RATIO- and SURFCO2-derived biosphere CO<sub>2</sub> fluxes for each Transcom region. They are defined as

$$p_{\text{CH}_4} = \left| x_{\text{CH}_4}^{\text{PROXY}} - x_{\text{CH}_4}^{\text{truth}} \right| - \left| x_{\text{CH}_4}^{\text{RATIO}} - x_{\text{CH}_4}^{\text{truth}} \right|,$$

$$p_{\text{CO}_2} = \left| x_{\text{CO}_2}^{\text{SURFCO2}} - x_{\text{CO}_2}^{\text{truth}} \right| - \left| x_{\text{CO}_2}^{\text{RATIO}} - x_{\text{CO}_2}^{\text{truth}} \right|, \quad (5)$$

where  $x$  denotes time series of monthly fluxes integrated over land Transcom regions. The subscripts indicate the tracer, and the superscripts indicate whether the fluxes refer to the truth or inversion estimates.  $p_{\text{CH}_4}$  and  $p_{\text{CO}_2}$  are arrays of 12-month time series for each Transcom land region. They are defined such that (1)  $p_{\text{CH}_4,i} > 0$  implies that RATIO is performing better than PROXY for CH<sub>4</sub> fluxes in the month  $i$ . (2)  $p_{\text{CO}_2,i} > 0$  implies that RATIO is performing better than SURFCO2 for CO<sub>2</sub> fluxes in month  $i$ . (3) For values of

$p_{\text{CH}_4,i}$  and  $p_{\text{CO}_2,i}$  less than 0, the reverse of (1) and (2) is true.

The upper panel of Fig. 10 shows  $p_{\text{CO}_2}$  and  $p_{\text{CH}_4}$  series for Boreal North America. The lower panel of Fig. 10 shows the cross-correlations between  $p_{\text{CH}_4}$  and  $p_{\text{CO}_2}$  for each Transcom land region. As can be seen, this value is above 0.7 (mean = 0.809) for all regions except for Australia (0.202) and Boreal Eurasia (0.539). A lack of surface measurements in these two regions can be the reason for the low correlation, as surface measurement stations are needed for good performance of both RATIO and PROXY (Sect. 4). Overall, we conclude that the relative performance of the proxy and ratio methods depends strongly on the relative performance of the surface-only and ratio CO<sub>2</sub> inversions.

#### 4 Discussion

We have developed the “ratio” method for TM5-4DVAR inversions system. It is an inversion system for assimilating the ratio of satellite-retrieved total columns of CH<sub>4</sub> and CO<sub>2</sub> along with surface measurements for constraining their surface fluxes. The main advantage of this method over the traditional proxy method is that it does not impose model-derived CO<sub>2</sub> concentrations as a hard constraint on the CH<sub>4</sub> flux optimization. Instead, our method allows optimization of CO<sub>2</sub> and CH<sub>4</sub> fluxes within a single consistent framework. This way we can benefit from proxy retrieval, which has proven to be highly efficient in reducing the errors due to light-path modification by atmospheric scattering, and at the same time, avoid projection of errors in  $X_{\text{CO}_2}^{\text{model}}$  on the inverted CH<sub>4</sub> fluxes. The method requires assimilation of surface measurements of CH<sub>4</sub> and CO<sub>2</sub> as an additional constraint, since a ratio alone is not a sufficient constraint for absolute values of CH<sub>4</sub> and CO<sub>2</sub> fluxes. For example, the inversions can reduce the modeled absolute CH<sub>4</sub> and CO<sub>2</sub> columns by the same factor and can still fit their ratio column to give a lower value of the cost function (Eq. 3).

The performance of the ratio method is tested in comparison with the traditional proxy method and surface-only inversions in an OSSE using the TM5-4DVAR atmospheric inversion system. Overall, we observe that the ratio method is capable of reproducing the true CH<sub>4</sub> and CO<sub>2</sub> fluxes better than the surface-only inversion. The performance of the ratio method in comparison to the proxy method varies among Transcom land regions. The performance of inversions assimilating satellite data in this study is optimistic compared to inversions using real observations as we have not introduced any systematic biases in our measurements. Also, as we do not filter out measurements taken in cloudy scenes and we use medium gain measurements in our inversion, we are optimistic about the satellite coverage in the tropics compared to real-life inversions. However, it is also true that satellite measurements are an important additional source of information about GHGs concentrations in these regions.

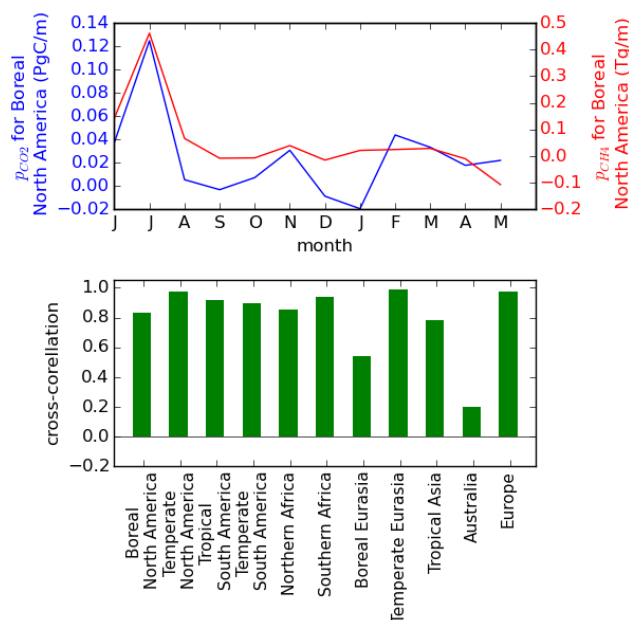


**Figure 10.** Top:  $p_{\text{CH}_4}$  and  $p_{\text{CO}_2}$  time series for Boreal North America. Bottom: cross-correlations between  $p_{\text{CH}_4}$  and  $p_{\text{CO}_2}$  for Transcom land regions (see Eq. 5).

The ratio method is a more complicated inversion to solve than a proxy inversion as it is a nonlinear inversion problem, and therefore the widely used CONGRAD optimizer cannot be used. In our setup, we use the M1QN3 optimizer, which is capable of handling the nonlinearity. However, inter-comparing inversions using different optimizers requires great attention as their mode of operation is mathematically different. For example, CONGRAD solves for the largest spatial and temporal scales in the first few iterations, gradually adjusting to finer scales in subsequent iterations. M1QN3 works in similar manner, however, it has a much slower convergence rate for the finer scales than CONGRAD. Hence, the overall convergence rate of M1QN3 is slower than CONGRAD, and to achieve the same gradient norm reduction takes more iterations (Krol et al., 2013).

Another drawback of M1QN3 compared to CONGRAD is that no information is obtained about posterior flux uncertainties. They are essential for inverse modeling applications using real data to quantify the constraints on the fluxes imposed by measurements. This is true, despite the fact that several important sources of uncertainty, such as transport model uncertainties, are difficult to account for. Furthermore, the accuracy of CONGRAD’s uncertainty approximation may be rather poor for large optimization problems, limiting its use. An alternative method for calculating posterior uncertainties is to use a Monte Carlo approach (Chevallier et al., 2007). This method can be applied also to inversions using M1QN3, although the method is computationally expensive. So far we have not investigated possible alternatives for M1QN3.

However, we would like to stress that there is a scope to find a more efficient optimizer for solving this nonlinear optimization problem, and future studies into the application of the ratio method should put an effort in this direction.

Fraser et al. (2014) developed a method for assimilating  $X_{\text{ratio}}$  in the MAP inversion setup coupled to the GEOS-Chem global 3-D atmospheric chemistry transport model. Similar to our findings, their OSSEs show that the assimilation of  $X_{\text{ratio}}$  along with surface measurements of CH<sub>4</sub> and CO<sub>2</sub> can reproduce the true fluxes. However, there are some important differences with our study:

1. We focus on a comparison between the proxy and ratio approach and also perform a CO<sub>2</sub> inversion using surface measurements for calculating the model-derived CO<sub>2</sub> fields used in the proxy approach. This way the propagation of errors from modeled CO<sub>2</sub> fields into proxy CH<sub>4</sub> measurements is also simulated. Instead, Fraser et al. (2014) add a constant or random bias to the  $X_{\text{ratio}}$  measurements.
2. Fraser et al. (2014) report posterior uncertainties of CH<sub>4</sub> and CO<sub>2</sub> fluxes derived from their  $X_{\text{ratio}}$  inversions. Although posterior flux uncertainties can in principle be derived from our method also, they are not reported here for computational reasons.
3. The ratio inversion system is weakly nonlinear. The Fraser et al. (2014) ratio inversions assume linearity. We do a nonlinear inversion using a suitable optimizer.

Now that we have demonstrated that the ratio method works in a synthetic environment, the next step is the application of the method to real satellite data. A first step in this direction is to validate GOSAT-observed  $X_{\text{CH}_4} : X_{\text{CO}_2}$  with TCCON. After that we plan to apply the ratio method to real satellite data, and compare the outcome with inversions using the GOSAT proxy and full-physics retrieval products. With improved constraints on the CO<sub>2</sub> side of the problem, as more spaceborne CO<sub>2</sub> measurements become available from GOSAT and OCO-2, the proxy method is expected to perform better for methane. In this case, one would expect the results of the proxy and ratio methods to converge. Whether or not this will really happen depends on the mutual consistency of the various data streams. The ratio method provides an internally consistent setup (i.e., within a single inversion system) to test this and to identify remaining biases. It should be noted that computationally, the ratio method has the advantage that it optimizes CH<sub>4</sub> and CO<sub>2</sub> fluxes together. This method can also be applied to other pairs of tracers, which are retrieved from close-by spectral ranges in the satellite measurement spectra. For example, CO total columns will be retrieved from TROPOMI (to be launched in 2016) using CH<sub>4</sub> as the proxy for atmospheric scattering, and there is a possibility that our ratio method can be applied successfully to this pair of tracers.

## 5 Conclusions

We developed a new inverse modeling method within the TM5-4DVAR inverse modeling framework for direct assimilation of satellite-observed ratios of total column CH<sub>4</sub> and CO<sub>2</sub>. The dual tracer inversion solves for surface fluxes of CH<sub>4</sub> and CO<sub>2</sub>. Our current implementation also assimilates surface measurements of CO<sub>2</sub> and CH<sub>4</sub> to further constrain the two tracer inverse problem. To deal with the weak non-linearity introduced by the optimization of tracer ratios we make use of the M1QN3 optimizer, instead of the CONGRAD optimizer, which was used so far for inversions using proxy retrievals. Although the optimization of the ratio inversion using M1QN3 is about a factor of 2 less efficient than the corresponding proxy inversion using CONGRAD, we nevertheless find satisfactory gradient norm reductions. We tested our method in an OSSE setup. We observe good convergence of posterior model columns toward the true ratio columns, and the ratio method is able to reproduce the true CH<sub>4</sub> and CO<sub>2</sub> fluxes from randomly perturbed prior fluxes.

We performed additional inversions in our OSSE setup to compare the performance of inversions using proxy and ratio retrievals from GOSAT. In addition, we compare the performances of these inversions, which also use surface measurements, with inversions that only use surface measurements. Additional inversions are performed to test the sensitivity of proxy inversions to the quality of the model-derived CO<sub>2</sub> concentrations, which are used to translate the retrieved tracer ratios into total columns of CH<sub>4</sub>. The performance of these inversions is evaluated by comparing the inversion-derived fluxes to a set of true fluxes from which the synthetic measurements were derived. The performance is assessed for monthly and annual fluxes integrated over the 11 Transcom land regions. Our results demonstrate that the estimation of CH<sub>4</sub> fluxes using the proxy inversion is sensitive to errors in the modeled-derived CO<sub>2</sub> concentrations.

We conclude that for most Transcom regions the ratio method is capable of reproducing the true seasonality and annually integrated CH<sub>4</sub> fluxes. However, it should be noted that the availability of surface measurements is important for good performance of the ratio method. The relative performance of the proxy and ratio methods shows a relationship with errors in CO<sub>2</sub>, with the ratio method performing better in regions where the CO<sub>2</sub> fluxes are poorly constrained. In our synthetic simulations, the ratio inversion is capable of improving the CO<sub>2</sub> fluxes compared with the use of CO<sub>2</sub> surface-only measurements, which explains why it outperforms the proxy method in certain regions. This points to the applicability of the ratio method for improving CO<sub>2</sub> fluxes in these regions. Further research is needed to test the performance of the ratio method in applications using real satellite data.

## Appendix A: M1QN3 and CONGRAD

We tested the convergence rate of CONGRAD and M1QN3 using the setup of PROXY described in Sect. 2.4. For this purpose, we carried out inversions with both optimizers for 30, 60 and 100 iterations and compared these to the standard inversion using 50 iterations. Figure A1 shows the corresponding posterior CH<sub>4</sub> flux departures from PROXY that are also shown in Fig. 7. We find that both the optimizers converge within 100 iterations. After 60 iterations, CONGRAD has already reached the solution, whereas M1QN3 shows slower convergence. Significant flux differences are found between the optimizers for inversions with 30 and 60 iterations. For CONGRAD, the difference between inversions with 50 and 60 iterations is negligible.

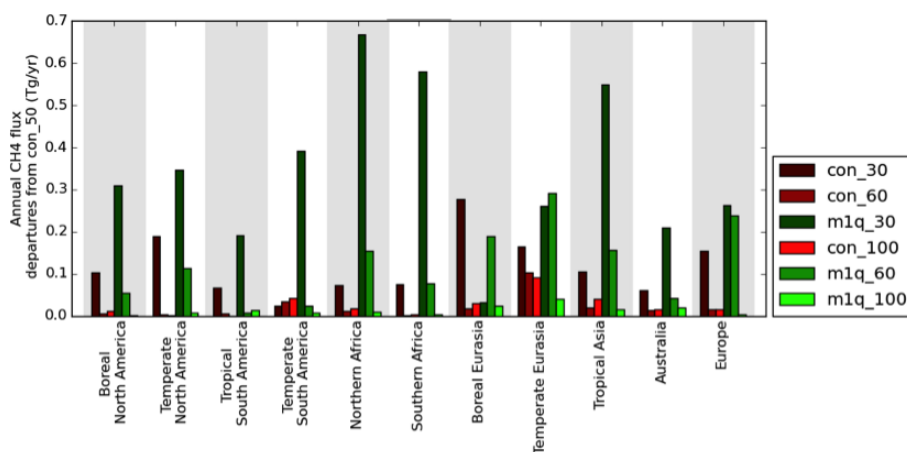


**Figure A1.** Absolute annual CH<sub>4</sub> flux departures of the inversion results from PROXY, which is run for 50 iterations using CONGRAD (see Fig. 7). The first part of label of each legend indicates the optimizer used for the inversion (m1q: M1QN3; con: CONGRAD), and the second part indicates number of iterations used.

**Acknowledgements.** This work is supported by the Netherlands Organization for Scientific Research (NWO), project number ALW-GO-AO/11-24. The computations were carried out on the Dutch national supercomputer Cartesius, and we thank SURFSara ([www.surfsara.nl](http://www.surfsara.nl)) for their support. We thank our data providers: NOAA/ESRL cooperative flask-sampling network surface observations were obtained from the website <http://www.esrl.noaa.gov/gmd/dv/ftpdata.html>; access to the GOSAT data was granted through the third GOSAT research announcement jointly issued by JAVA, NIES, and MOE. We would like to acknowledge Guillaume Monteil (IMAU) for his useful input.

Edited by: M. Heimann

## References

- Alexe, M., Bergamaschi, P., Segers, A., Detmers, R., Butz, A., Hasekamp, O., Guerlet, S., Parker, R., Boesch, H., Frankenberg, C., Scheepmaker, R. A., Dlugokencky, E., Sweeney, C., Wofsy, S. C., and Kort, E. A.: Inverse modelling of CH<sub>4</sub> emissions for 2010–2011 using different satellite retrieval products from GOSAT and SCIAMACHY, *Atmos. Chem. Phys.*, 15, 113–133, doi:10.5194/acp-15-113-2015, 2015.
- Basu, S., Guerlet, S., Butz, A., Houweling, S., Hasekamp, O., Aben, I., Krummel, P., Steele, P., Langenfelds, R., Torn, M., Biraud, S., Stephens, B., Andrews, A., and Worthy, D.: Global CO<sub>2</sub> fluxes estimated from GOSAT retrievals of total column CO<sub>2</sub>, *Atmos. Chem. Phys.*, 13, 8695–8717, doi:10.5194/acp-13-8695-2013, 2013.
- Basu, S., Krol, M., Butz, A., Clerbaux, C., Sawa, Y., Machida, T., Matsueda, H., Frankenberg, C., Hasekamp, O., and Aben, I.: The seasonal variation of the CO<sub>2</sub> flux over Tropical Asia estimated from GOSAT, CONTRAIL, and IASI, *Geophys. Res. Lett.*, 41, 1809–1815, doi:10.1002/2013GL059105, 2014.
- Bergamaschi, P. and Frankenberg, C.: Inverse modeling of global and regional CH<sub>4</sub> emissions using SCIAMACHY satellite retrievals, *J. Geophys. Res.*, 114, 1–28, doi:10.1029/2009JD012287, 2009.
- Bergamaschi, P., Frankenberg, C., Meirink, J. F., Krol, M., Dentener, F., Wagner, T., Platt, U., Kaplan, J. O., Körner, S., Heimann, M., Dlugokencky, E. J., and Goede, A.: Satellite cartography of atmospheric methane from SCIAMACHY on board ENVISAT: 2. Evaluation based on inverse model simulations, *J. Geophys. Res.*, 112, D02304, doi:10.1029/2006JD007268, 2007.
- Bousquet, P., Ciais, P., Miller, J. B., Dlugokencky, E. J., Hauglustaine, D. A., Prigent, C., Van der Werf, G. R., Peylin, P., Brunke, E.-G., Carouge, C., Langenfelds, R. L., Lathière, J., Papa, F., Ramonet, M., Schmidt, M., Steele, L. P., Tyler, S. C., and White, J.: Contribution of anthropogenic and natural sources to atmospheric methane variability, *Nature*, 443, 439–443, doi:10.1038/nature05132, 2006.
- Bousquet, P., Ringeval, B., Pison, I., Dlugokencky, E. J., Brunke, E.-G., Carouge, C., Chevallier, F., Fortems-Cheiney, A., Frankenberg, C., Hauglustaine, D. A., Krummel, P. B., Langenfelds, R. L., Ramonet, M., Schmidt, M., Steele, L. P., Szopa, S., Yver, C., Viovy, N., and Ciais, P.: Source attribution of the changes in atmospheric methane for 2006–2008, *Atmos. Chem. Phys.*, 11, 3689–3700, doi:10.5194/acp-11-3689-2011, 2011.
- Chevallier, F., Bréon, F.-M., and Rayner, P. J.: Contribution of the Orbiting Carbon Observatory to the estimation of CO<sub>2</sub> sources and sinks: Theoretical study in a variational data assimilation framework, *J. Geophys. Res.*, 112, D09307, doi:10.1029/2006JD007375, 2007.
- Cressot, C., Chevallier, F., Bousquet, P., Crevoisier, C., Dlugokencky, E. J., Fortems-Cheiney, A., Frankenberg, C., Parker, R., Pison, I., Scheepmaker, R. A., Montzka, S. A., Krummel, P. B., Steele, L. P., and Langenfelds, R. L.: On the consistency between global and regional methane emissions inferred from SCIAMACHY, TANSO-FTS, IASI and surface measurements, *Atmos. Chem. Phys.*, 14, 577–592, doi:10.5194/acp-14-577-2014, 2014.
- Dee, D. P., Uppala, S. M., Simmons, A. J., Berrisford, P., Poli, P., Kobayashi, S., Andrae, U., Balmaseda, M. A., Balsamo, G., Bauer, P., Bechtold, P., Beljaars, A. C. M., van de Berg, L., Bidlot, J., Bormann, N., Delsol, C., Dragani, R., Fuentes, M., Geer, A. J., Haimberger, L., Healy, S. B., Hersbach, H., Hólm, E. V., Isaksen, I., Kållberg, P., Köhler, M., Matricardi, M., McNally, A. P., Monge-Sanz, B. M., Morcrette, J.-J., Park, B.-K., Peubey, C., de Rosnay, P., Tavolato, C., Thépaut, J.-N., and Vitart, F.: The ERA-Interim reanalysis: configuration and performance of the data assimilation system, *Q. J. Roy. Meteor. Soc.*, 137, 553–597, doi:10.1002/qj.828, 2011.
- Dlugokencky, E. J., Bruhwiler, L., White, J. W. C., Emmons, L. K., Novelli, P. C., Montzka, S. A., Masarie, K. A., Lang, P. M., Crotwell, A. M., Miller, J. B., and Gatti, L. V.: Observational constraints on recent increases in the atmospheric CH<sub>4</sub> burden, *Geophys. Res. Lett.*, 36, L18803, doi:10.1029/2009GL039780, 2009.
- Errico, R. M.: What is an adjoint model?, *B. Am. Meteorol. Soc.*, 78, 2577–2591, doi:10.1175/1520-0477(1997)078<2577:WIAAM>2.0.CO;2, 1997.
- Ferretti, D. F., Miller, J. B., White, J. W. C., Etheridge, D. M., Lassey, K. R., Lowe, D. C., Macfarling Meure, C. M., Dreier, M. F., Trudinger, C. M., van Ommen, T. D., and Langenfelds, R. L.: Unexpected changes to the global methane budget over the past 2000 years, *Science*, 309, 1714–1717, doi:10.1126/science.1115193, 2005.
- Frankenberg, C., Meirink, J. F., van Weele, M., Platt, U., and Wagner, T.: Assessing methane emissions from global space-borne observations, *Science*, 308, 1010–1014, doi:10.1126/science.1106644, 2005.
- Fraser, A., Palmer, P. I., Feng, L., Boesch, H., Cogan, A., Parker, R., Dlugokencky, E. J., Fraser, P. J., Krummel, P. B., Langenfelds, R. L., O'Doherty, S., Prinn, R. G., Steele, L. P., van der Schoot, M., and Weiss, R. F.: Estimating regional methane surface fluxes: the relative importance of surface and GOSAT mole fraction measurements, *Atmos. Chem. Phys.*, 13, 5697–5713, doi:10.5194/acp-13-5697-2013, 2013.
- Fraser, A., Palmer, P. I., Feng, L., Bösch, H., Parker, R., Dlugokencky, E. J., Krummel, P. B., and Langenfelds, R. L.: Estimating regional fluxes of CO<sub>2</sub> and CH<sub>4</sub> using space-borne observations of XCH<sub>4</sub>:XCO<sub>2</sub>, *Atmos. Chem. Phys.*, 14, 12883–12895, doi:10.5194/acp-14-12883-2014, 2014.
- Gilbert, J. C. and Lemaréchal, C.: Some numerical experiments with variable-storage quasi-Newton algorithms, *Math. Program.*, 45, 407–435, doi:10.1007/BF01589113, 1989.

- Gurney, K., Law, R., Denning, A., Rayner, P., Baker, D., Bousquet, P., Bruhwiler, L., Chen, H., Ciais, P., Fan, S., Fung, I., Gloor, M., Heimann, M., Higuchi, K., John, J., Maki, T., Maksyutov, S., Ken, M., Peylin, P., Prather, M., Pak, B. C., Rander-son, J., Sarmiento, J., Taguchi, S., Takahashi, T., and Yuen, C.-W.: Towards robust regional estimates of CO<sub>2</sub> sources and sinks using atmospheric transport models, *Nature*, 415, 626–630, doi:10.1038/415626a, 2002.
- Hein, R., Crutzen, P. J., and Heimann, M.: An inverse modeling approach to investigate the global atmospheric methane cycle, *Global Biogeochem. Cy.*, 11, 43–76, doi:10.1029/96GB03043, 1997.
- Houweling, S., Kaminski, T., Dentener, F., Lelieveld, J., and Heimann, M.: Inverse modeling of methane sources and sinks using the adjoint of a global transport model, *J. Geophys. Res.*, 104, 26137–26160, 1999.
- Houweling, S., Krol, M., Bergamaschi, P., Frankenberg, C., Dlugokencky, E. J., Morino, I., Notholt, J., Sherlock, V., Wunch, D., Beck, V., Gerbig, C., Chen, H., Kort, E. A., Röckmann, T., and Aben, I.: A multi-year methane inversion using SCIAMACHY, accounting for systematic errors using TCCON measurements, *Atmos. Chem. Phys.*, 14, 3991–4012, doi:10.5194/acp-14-3991-2014, 2014.
- Kirschke, S., Bousquet, P., Ciais, P., Saunoy, M., Canadell, J. G., Dlugokencky, E. J., Bergamaschi, P., Bergmann, D., Blake, D. R., Bruhwiler, L., Cameron-Smith, P., Castaldi, S., Chevallier, F., Feng, L., Fraser, A., Heimann, M., Hodson, E. L., Houweling, S., Josse, B., Fraser, P. J., Krummel, P. B., Lamarque, J.-F., Langenfelds, R. L., Le Quééré, C., Naik, V., O’Doherty, S., Palmer, P. I., Pison, I., Plummer, D., Poulter, B., Prinn, R. G., Rigby, M., Ringeval, B., Santini, M., Schmidt, M., Shindell, D. T., Simpson, I. J., Spahni, R., Steele, L. P., Strode, S. A., Sudo, K., Szopa, S., van der Werf, G. R., Voulgarakis, A., van Weele, M., Weiss, R. F., Williams, J. E., and Zeng, G.: Three decades of global methane sources and sinks, *Nat. Geosci.*, 6, 813–823, doi:10.1038/ngeo1955, 2013.
- Krol, M., Houweling, S., Bregman, B., van den Broek, M., Segers, A., van Velthoven, P., Peters, W., Dentener, F., and Bergamaschi, P.: The two-way nested global chemistry-transport zoom model TM5: algorithm and applications, *Atmos. Chem. Phys.*, 5, 417–432, doi:10.5194/acp-5-417-2005, 2005.
- Krol, M. C., Hooghiemstra, P. B., van Leeuwen, T. T., van der Werf, G. R., Novelli, P. C., Deeter, M. N., Aben, I., and Röckmann, T.: Correction to “Interannual variability of carbon monoxide emission estimates over South America from 2006 to 2010”, *J. Geophys. Res.-Atmos.*, 118, 5061–5064, doi:10.1002/jgrd.50389, 2013.
- Kuze, A., Suto, H., Nakajima, M., and Hamazaki, T.: Thermal and near infrared sensor for carbon observation Fourier-transform spectrometer on the Greenhouse Gases Observing Satellite for greenhouse gases monitoring, *Appl. Optics*, 48, 6716–6733, 2009.
- Lanczos, C.: An iteration method for the solution of the eigenvalue problem of linear differential and integral operators, *J. Res. Nat. Bur. Stand.*, 45, 255, doi:10.6028/jres.045.026, 1950.
- Meirink, J. F., Bergamaschi, P., and Krol, M. C.: Four-dimensional variational data assimilation for inverse modelling of atmospheric methane emissions: method and comparison with synthesis inversion, *Atmos. Chem. Phys.*, 8, 6341–6353, doi:10.5194/acp-8-6341-2008, 2008.
- Monteil, G., Houweling, S., Dlugokencky, E. J., Maenhout, G., Vaughn, B. H., White, J. W. C., and Rockmann, T.: Interpreting methane variations in the past two decades using measurements of CH<sub>4</sub> mixing ratio and isotopic composition, *Atmos. Chem. Phys.*, 11, 9141–9153, doi:10.5194/acp-11-9141-2011, 2011.
- Monteil, G., Houweling, S., Butz, A., Guerlet, S., Schepers, D., Hasekamp, O., Frankenberg, C., Scheepmaker, R., Aben, I., and Röckmann, T.: Comparison of CH<sub>4</sub> inversions based on 15 months of GOSAT and SCIAMACHY observations, *J. Geophys. Res.-Atmos.*, 118, 11807–11823, doi:10.1002/2013JD019760, 2013.
- Müller, J.-F. and Stavrakou, T.: Inversion of CO and NO<sub>x</sub> emissions using the adjoint of the IMAGES model, *Atmos. Chem. Phys.*, 5, 1157–1186, doi:10.5194/acp-5-1157-2005, 2005.
- Myhre, G., Shindell, D., Bréon, F.-M., Collins, W., Fuglestedt, J., Huang, J., Koch, D., Lamarque, J.-F., Lee, D., Mendoza, B., Nakajima, T., Robock, A., Stephens, G., Takemura, T., and Zhang, H.: Anthropogenic and Natural Radiative Forcing, in: *Climate Change 2013: The Physical Science Basis. Contribution of Working Group I to the Fifth Assessment Report of the Intergovernmental Panel on Climate Change*, Cambridge University Press, Cambridge, UK and New York, NY, USA, 2013.
- Nisbet, E. G., Dlugokencky, E. J., and Bousquet, P.: Methane on the rise—again, *Science*, 343, 493–495, doi:10.1126/science.1247828, 2014.
- Peters, W., Jacobson, A. R., Sweeney, C., Andrews, A. E., Conway, T. J., Masarie, K., Miller, J. B., Bruhwiler, L. M. P., Pétron, G., Hirsch, A. I., Worthy, D. E. J., van der Werf, G. R., Rander-son, J. T., Wennberg, P. O., Krol, M. C., and Tans, P. P.: An atmospheric perspective on North American carbon dioxide exchange: CarbonTracker, *P. Natl. Acad. Sci. USA*, 104, 18925–18930, doi:10.1073/pnas.0708986104, 2007.
- Schepers, D., Guerlet, S., Butz, A., Landgraf, J., Frankenberg, C., Hasekamp, O., Blavier, J.-F., Deutscher, N. M., Griffith, D. W. T., Hase, F., Kyro, E., Morino, I., Sherlock, V., Sussmann, R., and Aben, I.: Methane retrievals from Greenhouse Gases Observing Satellite (GOSAT) shortwave infrared measurements: Performance comparison of proxy and physics retrieval algorithms, *J. Geophys. Res.*, 117, D10307, doi:10.1029/2012JD017549, 2012.
- Spahni, R., Chappellaz, J., Stocker, T. F., Loulergue, L., Hausamann, G., Kawamura, K., Flückiger, J., Schwander, J., Raynaud, D., Masson-Delmotte, V., and Jouzel, J.: Atmospheric methane and nitrous oxide of the Late Pleistocene from Antarctic ice cores, *Science*, 310, 1317–1321, doi:10.1126/science.1120132, 2005.
- Taylor, K. E.: Summarizing multiple aspects of model performance in a single diagram, *J. Geophys. Res.*, 106, 7183–7192, 2001.